Autocrine control of glioma cells adhesion and migration through IRE1α-mediated cleavage of SPARC mRNA

Nicolas Dejeans[1,2,‡], Olivier Pluquet[1,2,*,‡], Stéphanie Lhomond[1,2], Florence Grise[1,2], Marion Bouchecareilh[1,2], Amélie Juin[1,2], Maud Meynard-Cadars[1,2], Aurélien Bidaud-Meynard[1,2], Catherine Gentil[3], Violaine Moreau[1,2], Frédéric Saltel[1,2] and Eric Chevet[1,2,§]

[1]INSERM U1053, 146 rue Léo Saignat, 33076 Bordeaux, France
[2]Université Bordeaux-Segalen, 146 rue Léo Saignat, 33076 Bordeaux, France
[3]TIERS-MIP, Faculté de médecine de Purpan, 37 allées Jules Guesde, 31073 Toulouse, France

*Present address: Institut de Biologie de Lille, CNRS UMR8161/Universités Lille 1 et Lille 2/Institut Pasteur de Lille, 1, rue du Pr. Calmette, BP 447, 59021 Lille, France
‡These authors contributed equally to this work
§Author for correspondence (eric.chevet@u-bordeaux2.fr)

Accepted 28 May 2012
Journal of Cell Science 125, 4278–4287

doi: 10.1242/jcs.099291

Summary

The endoplasmic reticulum (ER) is an organelle specialized for the folding and assembly of secretory and transmembrane proteins. ER homeostasis is often perturbed in tumor cells because of dramatic changes in the microenvironment of solid tumors, thereby leading to the activation of an adaptive mechanism named the unfolded protein response (UPR). The activation of the UPR sensor IRE1α has been described to play an important role in tumor progression. However, the molecular events associated with this phenotype remain poorly characterized. In the present study, we examined the effects of IRE1α signaling on the adaptation of glioma cells to their microenvironment. We show that the characteristics of U87 cell migration are modified under conditions where IRE1α activity is impaired (DN_IRE1). This is linked to increased stress fiber formation and enhanced RhoA activity. Gene expression profiling also revealed that loss of functional IRE1α signaling mostly resulted in the upregulation of genes encoding extracellular matrix proteins. Among these genes, *Sparc*, whose mRNA is a direct target of IRE1α endoribonuclease activity, was in part responsible for the phenotypic changes associated with IRE1α inactivation. Hence, our data demonstrate that IRE1α is a key regulator of SPARC expression in vitro in a glioma model. Our results also further support the crucial contribution of IRE1α to tumor growth, infiltration and invasion and extend the paradigm of secretome control in tumor microenvironment conditioning.

Key words: IRE1, Cell adhesion, cell migration, Endoplasmic reticulum, SPARC

Introduction

The endoplasmic reticulum (ER) plays an essential role in maintaining the maturation and folding of secreted and transmembrane proteins. Disruption of normal ER functions upon various physiological conditions faced by solid tumors such as hypoxia or glucose deprivation, leads to the accumulation of misfolded proteins and the subsequent activation of an evolutionarily conserved signaling pathway named the unfolded protein response (UPR) (Schröder and Kaufman, 2005). UPR signaling induces translation attenuation and activation of specific gene expression programs aiming at reducing the protein load in the ER and at increasing ER folding and clearance capacity, respectively. As part of this mechanism, IRE1α, which is an ER stress sensor and an ER-resident kinase/endoribonuclease, promotes the splicing of *Xbp1* mRNA, thereby resulting in the synthesis of a potent transcription factor, and the subsequent transcriptional activation of specific genes involved in restoring ER homeostasis (Calfon et al., 2002; Yoshida et al., 2003). Recently IRE1α has also been shown to contribute to mRNA degradation through a process named Regulated IRE1 Dependent Decay of mRNA (RIDD) (Hollien et al., 2009). Connections between UPR signaling and human diseases have been established for instance with pathologies such as diabetes or cancer (Marciniak and Ron, 2006; Moenner et al., 2007). An increasing body of evidences indicates a functional link between IRE1α and tumor growth/progression. Indeed, impairing IRE1α signaling in human glioma cells reduced tumor growth and angiogenesis both in vitro and in vivo through mechanisms dependent on ischemia-induced VEGF expression (Auf et al., 2010; Drogat et al., 2007). The IRE1α substrate *Xbp1* has been shown to be necessary for tumor growth in vivo without affecting VEGF expression, suggesting that IRE1α mediates its angiogenic properties independently of the XBP1 pathway (Romero-Ramirez et al., 2004). Moreover, several reports also showed that XBP1 is overexpressed in human cancers (Shuda et al., 2003) and that constitutive expression of its spliced form is sufficient to promote multiple myeloma in vivo (Carrasco et al., 2007). Recently, a large-scale sequencing analysis of somatic mutations present in the kinome of a wide variety of human cancers revealed a high prevalence of mutations in the IRE1α gene (Greenman et al., 2007). However, the precise mechanisms by which wild-type or mutant IRE1α contribute to cancer development/progression

independently of the activation of other branches of the UPR, remains to be fully characterized. We have previously shown that IRE1α-deficient cell (DN_IRE1)-derived tumors had a different shape and spatial organization (Auf et al., 2010; Drogat et al., 2007). These changes were also accompanied by a decrease of the growth rate and a highly infiltrative and mesenchymal tumor phenotype. The goal of the present study was to better characterize the molecular pathways by which IRE1α can impact on glioma characteristics.

Herein, using different in vitro approaches, we have examined the effects of IRE1α inactivation on cell migration and cell adhesion in U87 glioma cells. We show that migration is increased in DN_IRE1 cells through the upregulation of the extracellular matrix protein SPARC. In addition, we demonstrate that IRE1α directly regulates *Sparc* mRNA expression at the post-transcriptional level, thereby contributing to auto/paracrine SPARC signaling in tumor cells. Our data reveal an emerging role of IRE1α in the control of tumor cell adhesion and migration.

Results

Loss of IRE1α activity correlates with changes in U87 glioma cells attachment and migration properties

To characterize the molecular and cellular mechanisms responsible for IRE1-dependent modulation of cancer cell proliferation and migration in vivo (Auf et al., 2010; Drogat et al., 2007), we tested the effect of the expression of a well characterized dominant negative form of IRE1α (DN_IRE1) (Auf et al., 2010; Drogat et al., 2007; Nguyên et al., 2004) (supplementary material Fig. S1A) on U87 cells proliferation, adhesion and invasion ability (Fig. 1). Alteration of IRE1α signaling was confirmed by the weak induction of *Xbp1* mRNA splicing in response to various ER stress inducers (Fig. 1A), as previously described (Drogat et al., 2007; Lee et al., 2002; Papandreou et al., 2011; Welihinda et al., 1998).

As expected, DN_IRE1 cells proliferation rate was lower than that of empty vector expressing cells (EV; Fig. 1B) and the number of migrating cells was significantly higher than in EV cells (Fig. 1C; supplementary material Fig. S1B). In addition, adhesion of DN_IRE1 cells was also increased on both collagen matrices and Matrigel (Fig. 1D). However, both cell lines exhibited similar invasion properties in Matrigel (supplementary material Fig. S1C). As the features of U87 cells characterized in the orthotopic tumor model (Auf et al., 2010; Drogat et al., 2007) presented some specificities that were not recapitulated in the experiments presented in Fig. 1, another model was developed to investigate cell adhesion and migration properties of DN_IRE1 cells. To this end, a neurosphere model was used to mimic the U87 EV and DN_IRE1 cells phenotypes previously described in vivo. As shown in Fig. 2A, the expression of DN_IRE1 resulted in a delay in neurosphere formation and in a decrease of the size they reached. This phenomenon was most likely due to differences in cell growth (Fig. 1B) and cell–cell adhesion properties existing between EV and DN_IRE1 cells. To further compare the migration properties of DN_IRE1 and EV cells, neurospheres of the same size were allowed to adhere, and both neurosphere dissociation and cell migration abilities were monitored across time. Cell number in both types of neurospheres plated on glass slides was also counted and was similar in EV and DN_IRE1 neurospheres (not shown). Forty-eight hours after seeding, EV neurospheres remained compact and homogenous whereas DN_IRE1 neurospheres appeared flattened and dissociated (Fig. 2B). Interestingly, the mode of cell migration appeared to be different for both cell lines. Indeed, DN_IRE1 cells presented a more collective and organized migration, in contrast to EV cells, which migrated in a stochastic/individual manner (Fig. 2B). Both the dissociation capacity of

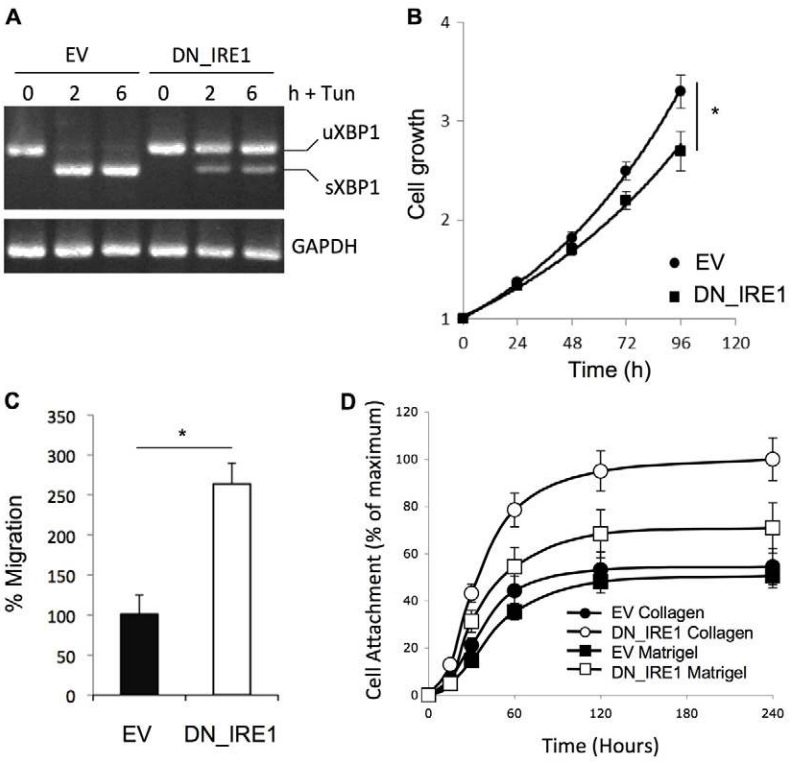

Fig. 1. Impairment of IRE1α signaling alters U87 cells migration, adhesion and proliferation properties. (**A**) Biochemical characterization of U87 cells expressing an empty vector (EV) or a dominant-negative form of IRE1α (DN_IRE1) for the splicing of *Xbp1* mRNA upon Tunicamycin (5 µg/ml)-induced ER stress. *Xbp1* mRNA splicing was evaluated by RT-PCR. The spliced (sXBP1) and unspliced (uXBP1) forms of XBP1 are indicated. (**B**) Cell growth was measured in normal serum conditions in EV and DN_IRE1 cells. (**C**) EV and DN_IRE1 cells were tested for migration in vitro in Transwell chambers as described in the Materials and Methods. The percentage of cells migrating through the Transwell inserts was determined. Results are expressed as percentage of the control (EV). (**D**) EV (closed symbols) and DN_IRE1 (open symbols) cells were assessed for their ability to attach to collagen (circles) or Matrigel (squares). After the indicated times, cell attachment was measured as a function of the absorbance (SRB assay at 492 nm). *$P<0.05$.

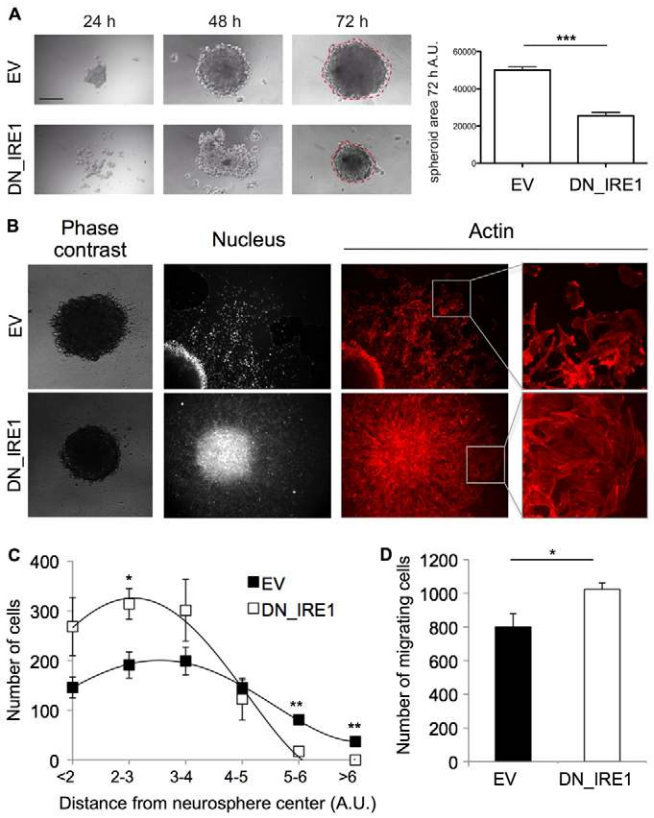

Fig. 2. Impairment of IRE1α signaling modulates neurosphere formation and migration capacity of U87 cells. (**A**) The ability of U87 cells expressing an empty vector (EV) or a dominant-negative form of IRE1α (DN_IRE1) to form neurospheres was evaluated as described in the Materials and Methods. 24, 48 and 72 h after seeding, photos were taken and after 72 h the neurosphere surface was measured using the ImageJ software. (**B**) EV and DN_IRE1 neurospheres of the same size and number of cells were allowed to adhere on a 22-mm glass coverslip and cell migration was studied for 48 h. Phase-contrast (4 h after neurosphere seeding) images and nuclear and F-actin stainings (48 h after seeding) are shown. (**C**) The distance achieve by all the cells escaping the neurosphere bulk was measured using nucleus staining and an ImageJ macro, and the number of cells travelling less than 2, 3–4, 4–5, 5–6 and more than 6 arbitrary unit (A.U.) was estimated. (**D**) Quantification of cells migrating from the neurosphere bulk (*P<0.05; **P<0.01).

DN_IRE neurospheres and the migration mode of the DN_IRE1 cells were reflected by the fact that more DN_IRE1 cells were migrating compared to EV cells, but the former appeared to migrate to a relatively shorter distance from the neurosphere center (Fig. 2C,D). Taken together, these data support the ability of IRE1α activity to regulate tumor cell features, including growth, migration and adhesion properties. Moreover, these data are consistent with those observed in vivo where DN_IRE1 cell-derived tumors were smaller, exhibited extensive tumor cell infiltration in the surrounding normal tissue than EV cell-derived tumors and were also tightly associated to the abluminal site of blood vessels without apparent penetration (Auf et al., 2010; Drogat et al., 2007).

As observed in Fig. 2B, the global organization of actin cytoskeleton was modified in DN_IRE1 cells. In this organization, stress fibers and focal adhesions constitute a contractile apparatus that allows cell attachment to the extracellular matrix through the plasma membrane and focal adhesions (Pellegrin and Mellor, 2007). Furthermore, these structures are known to constitute major cellular elements in the ability of cells to migrate. Considering these observations, we further examined the organization of the actin cytoskeleton and the associated adhesive contacts using immunofluorescence microscopy. We observed more actin stress fibers/cables in DN_IRE1 compared to control (EV) cells (Fig. 3A). This was accompanied by a gain of focal adhesions as illustrated by vinculin or paxillin staining (Fig. 3A; and quantified in Fig. 3B). In this context the small GTPase Rho represents one of the main regulators of actin stress fibers formation in adherent cells through activation of its effector protein Rho kinase (Ridley et al., 1999; Ridley et al., 1992). This led us to test whether RhoA activation was altered in DN_IRE1 cells compared to EV cells using commercially available kits (see Materials and Methods). Impairment of IRE1α activity led to significant basal activation of RhoA as assessed by using the G-LISA^{TM} assay (Fig. 4A). The role of RhoA as the main regulator of stress fiber formation was then confirmed in DN_IRE1 cells using either the pharmacological Rho-kinase inhibitor Y-27632 or RhoA

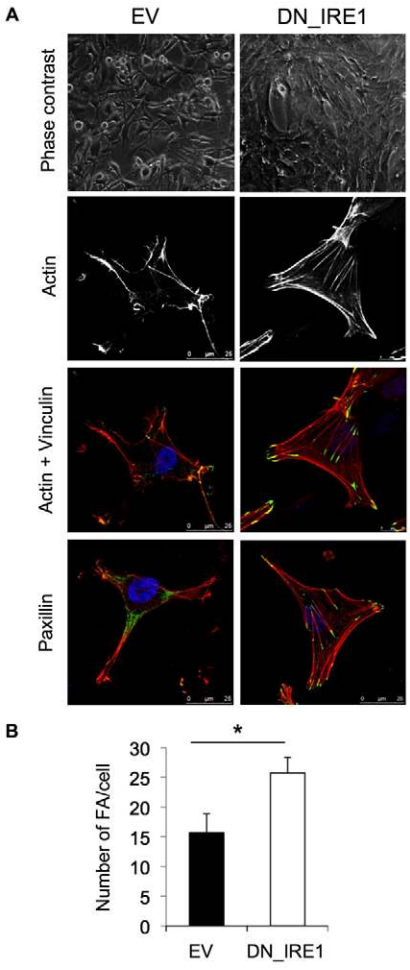

Fig. 3. Impairment of IRE1α signaling leads to F-actin cytoskeleton and cell architecture remodeling. (**A**) Phase-contrast analysis, phalloidin staining of F-actin and immunofluorescence analysis of vinculin and paxillin of EV and DN_IRE1 cells. (**B**) Measurement of focal adhesions (FA) in EV and DN_IRE1 cells as determined using vinculin staining (*P<0.05).

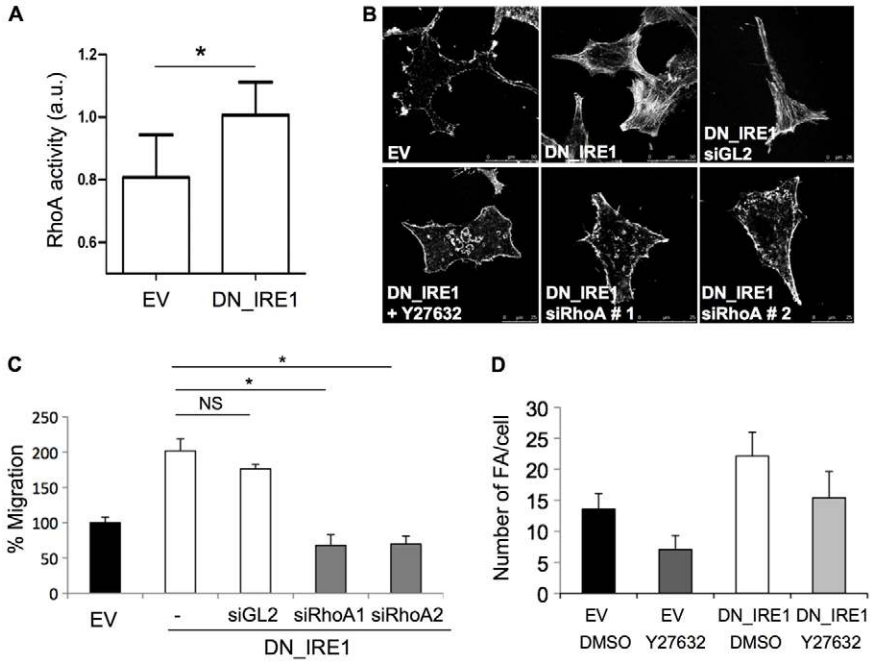

Fig. 4. Impairment of IRE1α signaling alters RhoA activation and cell adhesion properties in U87 cells. (**A**) RhoA activation in U87 EV and DN_IRE1 cells (measured as described in the Materials and Methods; *$P<0.05$). (**B**) EV and DN_IRE1 cells were either subjected to RhoA silencing by two different siRNAs (named no. 1 and no. 2) as well as a non-target luciferase siRNA (GL2) as a control, for 48 h or they were treated with the Rho Kinase inhibitor Y-27632 (10 μM) for 4 h. Fluorescence microscopy using phalloidin to stain F-actin was then performed on both cell lines. (**C**) Cells were subjected to RhoA silencing by the two different siRNAs as well as a non-target luciferase siRNA (GL2) as a control, for 48 h, and were tested for migration in vitro in Transwell assays. Migration was determined as in Fig. 1C (*$P<0.05$; NS, non-significant). (**D**) The number of focal adhesions was determined as described in the Materials and Methods in EV and DN_IRE1 cells treated with Y-27632 (10 μM) or DMSO for 24 h. A two-way ANOVA revealed a statistical difference between the DMSO and Y27632 conditions ($P<0.05$) and between the EV and DN_IRE1 cell types ($P<0.05$).

silencing strategies (supplementary material Fig. S2A) followed by immunofluorescence analyses. As shown in Fig. 4B, targeting RhoA signaling using either pharmacological or siRNA-based silencing strategies was sufficient to inhibit/prevent stress fiber formation in DN_IRE1 cells. This observation was also supported by the evaluation of the impact of RhoA silencing or Y-27632 treatment on U87 EV and DN_IRE1 cell migration capacity and focal adhesion number (Fig. 4C,D). In Fig. 4D, a two-way ANOVA statistical analysis revealed that both pharmacological treatment (Y27632) and expression of DN_IRE1 impacted on focal adhesion number per cell ($P<0.05$). These experiments showed that targeting RhoA expression or activity was sufficient to counteract DN_IRE1 cells migration ability and, in a same way, their increased focal adhesion number. This was also confirmed by measuring the impact of Y-27632 on the phosphorylation of the focal adhesion kinase (FAK), another focal adhesion marker (supplementary material Fig. S2B). Taken together, these results demonstrate that loss of IRE1α activity influences U87 cells attachment and migration properties by involving the small GTPase RhoA.

Gene expression profiling in EV and DN_IRE1 cells revealed differential expression of genes encoding extracellular matrix proteins

One of the major roles of IRE1α is to control the expression of membrane or secreted proteins coding genes through its capacities to splice the *Xbp1* mRNA or by directly cleaving a set of mRNA. Considering this, we hypothesized that DN_IRE1 cells might present modulations of the expression of mRNA encoding secretory or trans-membrane proteins in favor of an increase in adhesion and migration processes. To address this question, we compared mRNA expression profiles in control (EV; clone T1P5) and DN_IRE1 (clone 1C5) cells subjected or not to different ER stress inducing agents and thus IRE1α activators: glucose (−Glu) or glutamine (−Gln) deprivation, hypoxia (Hx) or tunicamycin (Tun) exposure. The data sets were deposited at the NCBI Gene Expression Omnibus GSE27306. Principal Component Analysis (PCA) was applied to visualize correlations in the control and DN_IRE1 transcriptional profiles. Fig. 5A illustrates that DN_IRE1 cells could be distinguished using the first two principal components, which account for 53% of total variation. DN_IRE1 cell populations were separated from control cells populations along the first principal component. We also noted that cultures performed under hypoxia (Hx) produced gene expression profiles that were separated from the other stress and basal culture conditions which showed intermediates positions along the second principal component. Other principal components did not display any information. This indicated that EV and DN_IRE1 populations subjected to Hx were associated with distinct transcriptional profiles, with some similarities in their gene expression. In contrast, the transcriptional profile of genes modulated in others control conditions showed very little overlap with profiles seen in others DN_IRE1 conditions.

To extract more information from these data, the PCA was applied by considering genes as individuals (Fig. 5B). The two first principal components accounted for 97% of the total variation. Fig. 5B shows genes that presented the most elevated mean between the different conditions along the first principal component and indicates the comparison of individual gene expression levels. The second principal component is built around genes that showed the biggest differences between samples from control and DN_IRE1 cells. PCA dimension 2 graphically shows the split between control and DN_IRE1 cells. The top 50 probe sets both positively and negatively regulated (corresponding to 40 genes; supplementary material Table S1) were subjected to functional annotation. The Kyoto Encyclopedia of Genes and Genome (KEGG), a compendium of genes annotated and organized by signaling pathway (Ogata et al., 1998), was used for this purpose (Fig. 5C). This revealed that both the ECM–receptor interaction and the focal adhesion signaling pathways were enriched in the DN_IRE1 signature, thus reinforcing our initial phenotypic observations.

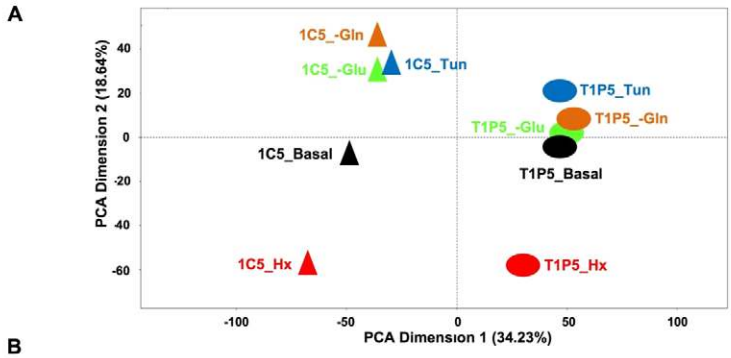

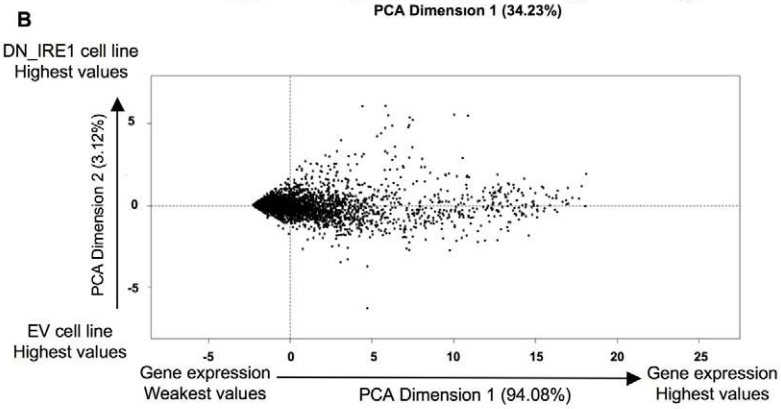

C

ID	Term	P value
4512	ECM-Receptor Interaction	0,00022
4510	Focal Adhesion	0,0058
4514	Cell Adhesion Molecules	0,086
0760	Nicotimide and nicotinamide metabolisms	0,086

Fig. 5. Transcriptional profiles of EV and DN_IRE1α cells revealed substantial differences in genes encoding extracellular matrix proteins. (**A**) Principal component analysis (PCA) of transcriptional profiles of EV (T1P5 clone) and DN_IRE1 cells (1C5 clone). The two-dimensional scatter plot shows the first two principal components of the analysis of 6078 genes. Data points from individual experimental conditions were represented using different shapes (triangles represent DN_IRE1 U87 cells, circles represent control U87 cells; Hx: hypoxia 0.1% for 16 h; -Glu: glucose deprivation for 16 h; -Gln: glutamine deprivation for 16 h; Tun: tunicamycin 1 μg/ml for 16 h). (**B**) Plot of individual genes that were significantly differentially expressed between EV and DN_IRE1 cells (all conditions combined). The top 50 probe-sets contributing the most to differences between EV and DN_IRE1 cells are listed in supplementary material Table S1. (**C**) Over-represented molecular pathways and functional annotation of the gene list in supplementary material Table S1 using KEGG pathway analysis.

IRE1α signaling regulates migration of U87 cells by downregulating Sparc mRNA expression

Based on the above-mentioned data, we further analyzed the list of genes identified through gene expression profiling (supplementary material Table S1) and selected genes that were i) overexpressed in DN_IRE1 cells, ii) involved in the modulation of cellular microenvironment and iii) functionally related to ER stress signaling. Based on these selection criteria, we selected SPARC. SPARC/Osteonectin is a matrix-associated protein that elicits changes in cell shape, inhibits cell-cycle progression and influences the synthesis of extracellular matrix (ECM) (Brekken and Sage, 2001; Chlenski and Cohn, 2010). Moreover, SPARC was a good candidate to explain the in vivo DN_IRE1 expressing tumor phenotype previously observed. Indeed, it was shown that SPARC overexpression delays tumor growth and promotes invasion in a rat glioma model (Kunigal et al., 2006; Rempel et al., 2001). Adding to that, *Sparc* mRNA was identified as a RIDD substrate that led to the repression of its expression through an internal cleavage (Hollien and Weissman, 2006). Using quantitative real-time PCR and semi-quantitative PCR we showed that SPARC mRNA was overexpressed in different clones of DN_IRE1 expressing cells compared to control cells under basal conditions and upon ER stress (Fig. 6A,B). As previously demonstrated (Hollien et al., 2009; Hollien and Weissman, 2006), we found that ER stress inducers (tunicamycin and dithiothreitol; DTT) were able to decrease *Sparc* mRNA in an IRE1α dependent manner in our glioma model (Fig. 6B). Moreover, siRNA-mediated IRE1α silencing in glioma cells led to increase *Sparc* mRNA expression (Fig. 6C; supplementary material Fig. S2C). A recent study identified a conserved consensus IRE1α cleavage sequence located in stem-loop structures on mRNA (Oikawa et al., 2010). Based on this information, we found only one potential IRE1α-cleavage site within *Sparc* mRNA using the M-FOLD program (Fig. 6D). We then investigated whether *Sparc* mRNA was cleaved by IRE1α using an in vitro RNA cleavage assay as previously reported (Bouchecareilh et al., 2011a). Total RNA from U87 cells was subjected to the in vitro cleavage assay in the presence of GST–IRE1α. RT-PCR using primers overlapping or not the putative cleavage site were then performed to determine the *Sparc* mRNA levels (Fig. 6E). In vitro results indicated a strong decrease in *Sparc* mRNA expression corresponding to the cleaved amplicon only (1499–1709) whereas another region of *Sparc* mRNA (278–479) remained intact (Fig. 6E). These data indicate that IRE1α is responsible of *Sparc* mRNA cleavage, which will lead inevitably to its exonuclease-mediated degradation in a cellular context.

We next sought to investigate the consequences of IRE1α-mediated alteration of SPARC expression in U87 cells. To modulate *Sparc* mRNA expression in U87 cells, a siRNA-based approach was undertaken and SPARC expression was indeed efficiently silenced in both control (EV) and DN_IRE1 cells at both RNA and protein levels (Fig. 7A; supplementary material Fig. S2D). This strategy allowed us to almost completely suppress SPARC secretion in the extracellular medium (supplementary material Fig. S3A). To identify if SPARC overexpression was associated with RhoA activation and focal adhesion/stress fiber regulation, we measured FAK phosphorylation and RhoA

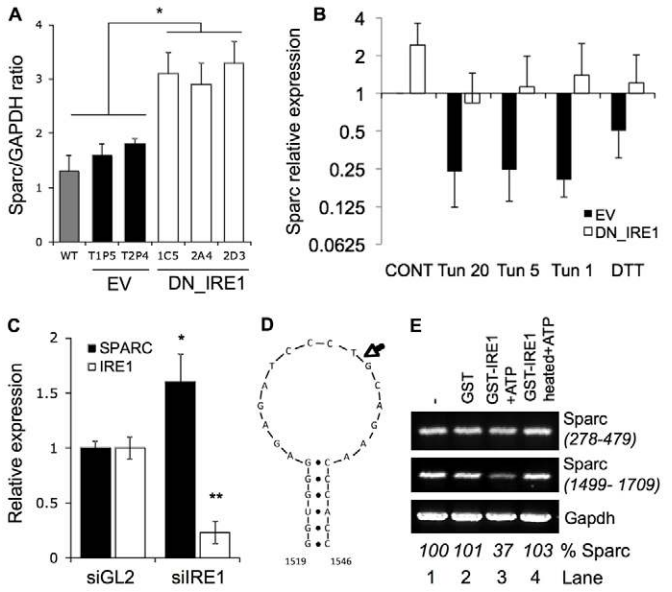

Fig. 6. IRE1α mediates the cleavage of *Sparc* mRNA. (**A**) *Sparc* mRNA expression in wild-type, EV (T1P5 and T2P4 clones) and DN_IRE1 (1C5, 2A4 and 2D3 clones) cells as quantified by quantitative RT-PCR. (**B**) *Sparc* mRNA levels were measured by quantitative RT-PCR and were normalized to beta-2 microglobulin (B2M) levels upon treatment with ER stress inducers including Tunicamycin (Tun, 20, 5 and 1 μg/ml, 24 h) or DTT (2 mM, 6 h). Results were normalized to the EV non-stressed condition. (**C**) siRNA-mediated attenuation of IRE1α expression (white bars) leads to enhanced *Sparc* mRNA expression (black bars). (**D**) Schematic representation of the IRE1α cleavage sites with secondary structures, predicted using M-FOLD. The cleavage site is indicated by an arrow. (**E**) In vitro RNA cleavage assay. Total RNA extracted from U87 cells was incubated with GST or GST–IRE1α-cyto in the presence of ATP for 2 h at 37℃. In the 'GST-IRE1 heated + ATP' condition, GST–IRE1α-cyto was heated to suppressed its activity, and used as a negative control. RT-PCR was then performed to determine *Sparc* and *Gapdh* mRNA levels. Quantifications are indicated as percentage of control (**P*<0.05).

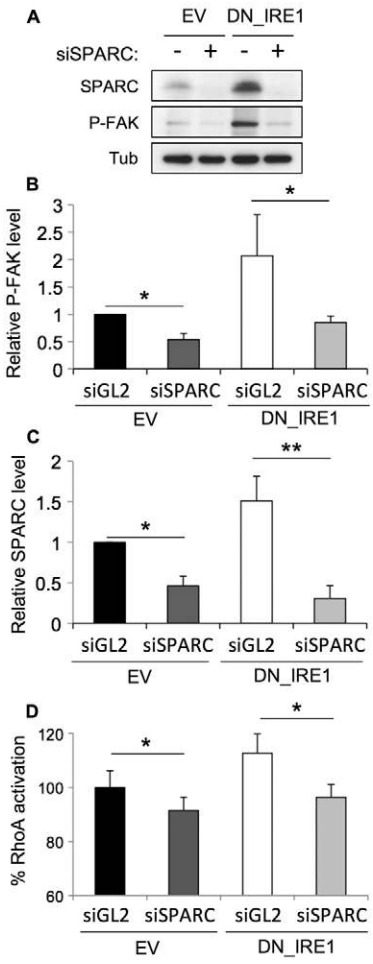

Fig. 7. IRE1α-mediated *Sparc* mRNA controls U87 architectural structure. (**A**) EV and DN_IRE1 cells were subjected to SPARC silencing by siRNA or non-target luciferase (GL2) silencing as a control. SPARC protein levels and FAK phosphorylation were evaluated by western blotting. Tubulin (Tub) was used as a loading control. (**B**,**C**). Relative quantification of SPARC protein levels and FAK phosphorylation. Values were normalized to tubulin levels. (**D**) EV and DN_IRE1 cells were subjected to SPARC silencing by siRNA or non-target luciferase (GL2) silencing as a control and were assessed for RhoA activation. (**P*<0.05; ***P*<0.01).

activation in EV or DN_IRE1 cells silenced or not for SPARC (Fig. 7). As expected, SPARC expression correlated perfectly with P-FAK (Fig. 7A–C) and with RhoA activation (Fig. 7D). To further test whether SPARC-mediated RhoA activation and FAK phosphorylation were associated with the migration/proliferation phenotype observed for DN_IRE1 cells, the capacity of EV and DN_IRE1 cells to form neurospheres and to migrate in Transwell assays was then studied (Fig. 8). First and as anticipated, siRNA-mediated downregulation of *Sparc* mRNA expression significantly increased the size of neurospheres after 72 h (Fig. 8A). Second, SPARC silencing altered the migration capacity of both EV and DN_IRE1 cells (Fig. 8B). Third, the use of SPARC blocking antibodies (Sweetwyne et al., 2004) in the medium of cultured cells led to a similar observation with the reduction of cell migration, thus suggesting an autocrine/paracrine mechanism of action (Fig. 8C). This demonstrated that the process of IRE1α-mediated control of U87 cells was SPARC-dependent and most likely occurred in an autocrine/paracrine fashion.

Discussion

In the present study, using a combination of cellular and molecular approaches we correlate the inhibition of IRE1α activity in glioma with alteration of tumor cells/extracellular matrix interactions. We show that the structure of the actin cytoskeleton is affected in IRE1α signaling deficient cells compared to control cells (Figs 2, 3), thereby indicating an alteration of cell's architecture and demonstrating an increase in focal adhesions number. Moreover, at the molecular level, transcriptional profiles indicated substantial differences between control and DN_IRE1 cells. Indeed a majority of genes modulated in DN_IRE1 cells encoded secreted proteins associated to the extracellular matrix or to cell adhesion (Fig. 5) such as collagen or fibronectin (supplementary material Table S1). Based on these analyses, we identify *Sparc* mRNA as an IRE1α-endoribonuclease regulated transcript relevant of our glioma model. *Sparc* encodes a matrix secretory protein that regulates the interaction of tumor cells with the extracellular matrix and impacts on their adhesion/migration properties through, among others, the activation of RhoA signaling (Figs 7, 8). These data led us to propose a model in which ER stress-mediated control of

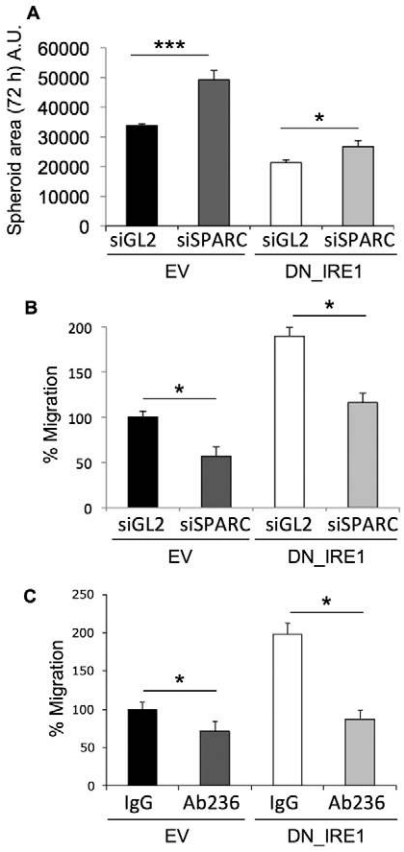

Fig. 8. Role of *Sparc* mRNA expression in DN_IRE1 cell migration and neurosphere formation. (**A**) Sizes of spheroids formed by incubating 2000 cells silenced or not for SPARC on an agar matrix for 72 h, as described in the Materials and Methods. (**B**) EV and DN_IRE1 cells were subjected to SPARC silencing by siRNA or non-target luciferase (GL2) silencing as a control and were tested for migration in vitro using Transwell assays. (**C**) EV and DN_IRE1 cells were exposed to SPARC blocking antibodies (ab236) added to the medium and were tested for migration in vitro using Transwell assays (*P<0.05; ***P<0.001).

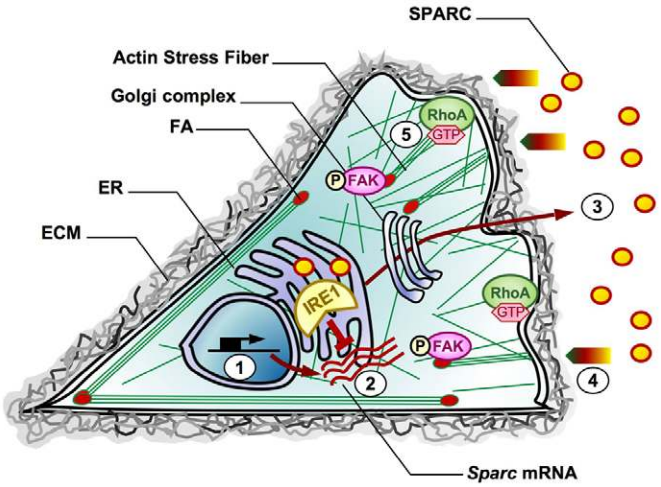

Fig. 9. Schematic representation of the mode of action of IRE1α signaling in gliomas leading to control of cell proliferation and migration. U87 wild-type cancer cells can still proliferate under challenging conditions through enhanced adaptability. In contrast, when IRE1α signaling is impaired, cell proliferation capacity is decreased, which is associated to the post-transcriptional derepression of *Sparc* mRNA expression (1 and 2). Secreted SPARC (3) will in turn, interact with the extracellular matrix (4) and consecutively enhanced cell migration, stress fiber formation and focal adhesion number through RhoA-dependent mechanisms (5). ECM, extracellular matrix; ER, endoplasmic reticulum; FA, focal adhesion.

Sparc mRNA expression could provide a selective advantage for tumor cells to adapt to challenging environments (Fig. 9).

Several reports have previously demonstrated that IRE1α mediates both the cleavage and the degradation of mRNA encoding secretory proteins independently of the *Xbp1* pathway (Hollien et al., 2009; Hollien and Weissman, 2006; Oikawa et al., 2010; Oikawa et al., 2007). Oikawa and colleagues identified a consensus sequence CU↓GCAG with IRE1α cleavage site present between the second and the third base and located in the loop portion of a stem loop structure, similar to those found in *Xbp1* mRNA (Yoshida et al., 2003; Yoshida et al., 2001). Interestingly, we found a sequence compatible with this consensus in *Sparc* mRNA and its in vitro cleavage by IRE1α was monitored by PCR (Fig. 6). Moreover, the *D. melanogaster* ortholog of *Sparc* mRNA was identified as an IRE1α substrate in a previous study (Hollien and Weissman, 2006). This reinforced the relevance of our observation and strongly suggested a link between ER stress signaling and tumor cells adhesion/migration processes.

High levels of *Sparc* mRNA have been correlated with cancer progression and poor prognosis, or in contrast, with tumor suppression depending of the cancer types (Podhajcer et al., 2008; Tai and Tang, 2008). As such, downregulation of SPARC by siRNA in invasive glioma cell lines, which were subsequently injected in an orthotopic mouse model, led to inhibition of infiltrating tumor cell dissemination (Seno et al., 2009). As well, in glioma, overexpression of SPARC inhibits cell proliferation both in vitro and in vivo (Podhajcer et al., 2008; Tai and Tang, 2008). When injected into immunodeficient rat brains, U87 cell-derived tumors overexpressing SPARC exhibited small tumor size with extensive tumor cell infiltrations compared to U87 control cell-derived tumors, which were bigger with a well delimited perimeter (Schultz et al., 2002). The latter phenotype presented therefore features similar to those observed in DN_IRE1 glioma cell-derived tumors (Auf et al., 2010; Drogat et al., 2007).

SPARC has been characterized as acting in matrix remodeling and cell migration processes. SPARC participates to survival, adhesion, migration, invasion in glioma cell lines (Arnold and Brekken, 2009). Both aggressiveness and migration capacity of cancer cells were shown to depend on SPARC concentration in the ECM, thereby making SPARC a target for therapies treating glioma invasion (Kunigal et al., 2006). Moreover, we observed an enhanced activation of RhoA in cells deficient for IRE1α signaling (Fig. 4). This is in agreement with data showing that RhoA is involved in the SPARC-induced migration of U87 cells (Kunigal et al., 2006) and is consistent with our previous work linking Rho GTPase signaling to the Unfolded Protein Response (Bouchecareilh et al., 2011b; Caruso et al., 2008). Moreover, SPARC expression has been previously described to increase U87 cell migration (Rempel et al., 2001). Furthermore, in our study, DN_IRE1 cells migration specific properties were also correlated with increased attachment to collagen and Matrigel

compared to EV cells (Fig. 1) and to the upregulation of the expression of extracellular matrix proteins (supplementary material Table S1). Interestingly Schultz and colleagues and Golembieski and Rempel found that the level of secreted SPARC controls the balance between tumor cells adherence and migration (Schultz et al., 2002; Golembieski and Rempel, 2002). They showed that, in contrast to low and high levels of SPARC expression, which promote tumor invasiveness, intermediate expression levels induce stronger adherence and a typical in vivo invasion as a bulk tumor along the corpus callosum. In our study, DN_IRE1 glioma cells presented some characteristics that could correspond to an intermediate level of SPARC expression. Indeed, DN_IRE1 expressing cells present elevated migration capacity, weak invasion ability and a migration profile more collective than that of EV expressing cells (Figs 1, 2; supplementary material Fig. S1).

SPARC downstream signaling regulating glioma migration was shown to involve HSP27 and p38MAPK (Golembieski et al., 2008) as well as the uPA–uPAR system (Kunigal et al., 2006), the TGF-beta (Francki et al., 2004) and integrins (Barker et al., 2005) signaling pathways or the SHC–RAF–ERK pathway (Thomas et al., 2010). As our initial phenotypic observations correlated with increased stress fiber formation and RhoA activity, we focused on this signaling pathway as a read out of SPARC secretion and activity. Our data suggest that secretion of SPARC and extracellular matrix proteins (collagen, fibronectin) may influence the local environment, resulting in enhanced glioma cell migration (supplementary material Table S1). Interestingly, we found that SPARC addition to the media (0.1 and 1 μg/ml, 24 h) was not sufficient to reproduce the DN_IRE1 effect on U87 cell migration or focal adhesion increase (not shown). However, we also found that SPARC blocking antibodies were sufficient to suppress the increase in DN_IRE1 expressing U87 cells migration capacity (Fig. 8C). With regard to these results, we might propose that SPARC overexpression is necessary but not sufficient to explain DN_IRE1 cells migration capacity. For instance, SPARC has been shown to enhance fibronectin-induced stress fiber formation and fibronectin matrix assembly (Barker et al., 2005). In our model, both fibronectin expression and SPARC levels were increased (supplementary material Table S1; Fig. 7A; supplementary material Fig. S3B), thereby suggesting a synergistic effect. We propose a model in which SPARC impacts on the cell interaction with its ECM and induces a range of signaling pathways to promote a general induction of stress fiber formation and increase in cell migration (Fig. 9).

Our data provide the first molecular connection between IRE1α signaling in the ER and tumor phenotypes. In Fig. 9, we propose a model that recapitulates our data in which impairing IRE1α signaling in glioma cells relieves the post-transcriptional repression of *Sparc* mRNA. This in turn leads to the modulation of cell migration properties through RhoA-dependent mechanisms. This model could be disease-relevant since *IRE1α* has been found mutated in a panel of human gliomas (Greenman et al., 2007; Parsons et al., 2008). Interestingly, two of these mutations, more precisely the Q780 (a stop mutant) and the S769F were recently found to result in the abrogation of IRE1α endoribonuclease activity (Xue et al., 2011). Hence, we propose that IRE1α activity may be modulated in these mutated human cancers, and therefore may contribute to tumor progression through, for instance, SPARC dependent processes.

Materials and Methods

Cell culture and treatments

U87 cells were grown in DMEM glutamax (Invitrogen, Carlsbad, CA, USA) supplemented with 10% FBS and antibiotics. U87 were stably transfected with pcDNA3/IRE1-NCK1, an expression vector encoding a cytoplasmic-defective IRE1α mutant). U87 cells were selected using 450 μg/ml G418 and several isolated clones were tested: T1P5 (referred as EV in the text) and T2P4 as empty vector and 1C5 (referred as DN_IRE1 in the text), 2A4 and 2D4 as IRE1 dominant negative expressing cell lines. For microarray experiments, tunicamycin (purchased from Calbiochem; Merck KGaA, Darmstadt, Germany) was used at 1 μg/ml for 16 h, hypoxic conditions were done at 1% in a Heraeus incubator BB-6060, glucose deprivation was performed by using DMEM F405 medium supplemented with 1% FBS and glutamine deprivation was done by using DMEM F405 medium supplemented with 1% FBS and glucose. RhoA inhibitor Y-27632 and DTT were purchased from Sigma (St Louis, MO, USA).

Western blotting

Antibodies against P-FAK and fibronectin were purchased from BD Transduction Laboratory (Oxford, UK), alpha-tubulin from Sigma (St Louis, MO, USA), RhoA from Santa Cruz Biotechnology (Santa Cruz, CA) and SPARC from Cell Signaling Technology (Danvers, MA). Anti-CNX antibodies were kindly given by John Bergeron (McGill University, Montreal, QC, Canada). SPARC extraction from cell culture media was performed by adding 75 μl of rehydrated Heparin Sepharose CL-6B (GE Healthcare, USA) to 5 ml of cell culture media containing 1% FBS. The solution was then incubated with agitation at 4°C for 4 h. The gel was then recovered by centrifugation and mixed with Laemmli sample buffer before western blotting.

Small Interfering RNA

Small interfering (si) RNAs were chemically synthesized (MWG) and transfected into U87 cells and derivatives (50 nmol) using Lipofectamine™ RNAiMAX (Invitrogen, Carlsbad, CA, USA) for 72 hrs according to the protocol of the manufacturer. Small interfering RNAs were designed against RhoA mRNA (5′-AAGAAGTCAA-GCATTTCTGTC-3′ or purchased from Applied Biosystems, Ambion, Carlsbad, CA, USA), against SPARC mRNA (5′-GAAGAUCCAUGAGAAUGAG-3′; 5′-ACACACAUUGCAGCUUCAA-3′; 5′-ACAAGACCUUCGACUCUUC-3′) or IRE1 mRNA (5′-GCGUCUUUUACUACGUAAU-3′) or purchased (for IRE1) from Dharmacon (Lafayette, CO, USA). As a control we used the GL2 siRNA sequence (5′-CGUACGCGGAAUACUUCGATT-3′) designed to target the firefly luciferase.

RhoA activity assay

RhoGTPase protein activity assay was performed by using the G-LISA™ RhoA Activation Assay Biochem Kit™ (Cytoskeleton Inc., CO, USA) according to the manufacturer's instructions.

Attachment assays

Plates (96-well) were coated with a filtered solution of 400 μg/ml collagen in PBS (Sigma, St Louis, MO, USA) or with Matrigel as previously described (Kunigal et al., 2006; Rempel et al., 2001). Rat tail collagen I was purchased from BD Bioscience and was coated on culture plates as recommended by the manufacturer. EV and DN_IRE1 cells (25,000 cells) were plated for time points 0, 15 and 30 min and 1, 2 and 4 hours. Medium and unattached cells were aspirated. Wells were washed with PBS and attached cells were fixed in 3% paraformaldehyde for 30 min, rinsed with PBS three times, and stained with Sulforhodamine B (SRB assay kit, Sigma, St Louis, MO, USA). Data were quantified by spectrophotometry at 492 nm. At time 0, no cell was attached to the substratum.

Immunofluorescence analyses

Cells grown on 12-mm coverslip (Rempel et al., 2001) were treated as indicated, washed with PBS, fixed with 4% paraformaldehyde for 15 min at room temperature, and then blocked with 5% BSA, PBS, 0.1% Triton X-100 for 1 h. Filamentous actin was visualized using phalloidin–FITC as previously described (Liu et al., 1999). Cortactin, paxillin, vinculin, cells were visualized as previously described (Moreau et al., 2003). Cells were incubated with primary antibodies for 16 h at 4°C, washed with PBS, and incubated for 1 h with FITC/TRITC conjugated secondary antibodies (Invitrogen, Carlsbad, CA, USA). To visualize the nucleus, cells were counterstained with 1 μg/mL 4,6-diamidino-2-phenylindole (DAPI, Sigma, St Louis, MO, USA). After mounting, cells were analyzed with a SP5 confocal microscope (Leica Microsystems, Mannheim, Germany).

Focal adhesion quantification

Quantification of focal adhesion was adapted from the method of Juin and colleagues (Juin et al., 2012). Confocal images of isolated cells were obtained using a SP5 confocal microscope (Leica Microsystems, Mannheim, Germany) by using a 63×/NA 1.4 Plan Neo-Fluar objective. Cell surface area was measured upon phalloidin staining, and vinculin staining was used as a focal adhesion

marker. We developed a macro with ImageJ software that allowed measurement of all required parameters of focal adhesions: number/cells and cell size (using the Feret diameter, the longest distance between any two points). At least 2000 focal adhesions were counted for each condition in three independent experiments and in a total of 180 to 280 cells. The results were expressed as the mean of the three experiments.

Migration and invasion assays

Cells were tested for migration and invasion abilities in vitro using 8 μm pores Transwell inserts (BD BioCoat^{TM}). The upper side of the Transwell inserts with 8 mm pores was either uncoated (migration) or coated (invasion) with Matrigel. U87 cells were added to the upper chamber at 25,000 cells per well in serum free medium. The lower portion of the chamber contained 1% serum as chemo attractant. After incubation for 16 h, the cells at the upper side were removed with a cotton swab. Filters were fixed with paraformaldehyde 3% for 30 min, and then the cells at the lower side were stained with Crystal Violet 0.1%. The level of migration and invasion was determined by counting cells in five randomly areas under a light microscope.

Neurospheres

Neurosphere formation experiments were performed by incubating 2000 cells by well in a 96-well plate previously coated with 50 μl of 1.5% agar gel. For neurosphere dissociation/migration, neurospheres of the same size (obtained by incubating 3000 and 6000 of EV and DN_IRE1 expressing cells, respectively) were put on a 22-mm coverslip and incubated for 48 h. Then, neurosphere were fixed with 4% paraformaldehyde for 20 min at room temperature. Cell actin (phalloidin-546) and nucleus (Hoechst) were stained and visualized as described in the Immunofluorescence analyses section with some modifications: after blockage, neurosphere cells were incubated 1 h with Hoechst and phalloidin-546. After mounting, cells were analyzed using a Zeiss epifluorescence microscope.

RNA cleavage assay

Total RNA (10 μg) from U87 was incubated with the cytoplasmic domain of human GST–IRE1α (5 μg) at 37℃ for the indicated times in a 5× buffer containing 250 mM Tris pH 7.5, 600 mM NaCl, 5 mM $MgCl_2$, 5 mM $MnCl_2$, 25 mM β-mercaptoethanol, supplemented with or without 10 mM ATP. As control, we used GST–IRE1α denatured by heating 10 min at 100℃. RT-PCR was performed using SPARC primers and GAPDH as internal control. IRE1α cleaved or uncleaved RNAs were used as a template for reverse transcription and PCR was then performed using SPARC primers. Secondary structure of *Sparc* mRNA was predicted using M-FOLD (http://mobyle.pasteur.fr/cgi-bin/portal.py?form=mfold).

Microarray experiments and analyses

Microarray assay and preprocessing analysis were performed in the microarray core facility of the Research Institute for Biotherapy at Montpellier using the standard Affymetrix protocol. Total RNA was extracted using Trizol (Invitrogen). RNA integrity was verified on an Agilent 2100 Bioanalyzer. For each of the samples, total RNA was reverse transcribed into cDNA, followed by in vitro transcription and biotin labeling to generate cRNA (Enzo Biochem, Farmingdale, NY, USA). The fragmented, biotin-labeled cRNA was hybridized to Human Genome U133 2.0 oligonucleotide arrays (Affymetrix, Santa Clara, CA, USA) containing approximately 22,000 probes. Microarrays were stained with streptavidin antibody and streptavidin–phycoerythrin in an Affymetrix Fluidics station. Arrays were scanned using a 3000 7G scanner. Row data were analyzed and principal components analysis (PCA) was carried out to highlight potential expression profiles within and across cell lines using R software version 2.8.0 (Gentleman et al., 2004). Spots for which the gene expression values were too low or not statistically significant were removed (6078 probesets were selected). Principal Component Analysis (PCA) builds a new coordinate system, which maximizes the variance in the data. The Principal Components (PCs) are linear combinations of the original variables X1, X2, …, Xz, chosen in such a way that PCA dimension 1 describes the largest fraction of variation in the data, and subsequent PCs describe maximal portions of the remaining variation. An essential requirement is that all PCs should be orthogonal to each other. Thus, only the first few PCs need to be considered to get a good overview of the data. In our datasets, the variables X1, X2, …, Xz represent our different cell conditions. The data of n objects (gene expression), each measured at m treatments or cell lines, can be written as an n by m matrix X. Before mapping the data, the samples in X were centered by subtracting their means and a biplot was then constructed. The Kyoto encyclopedia of Genes and Genomes (KEGG), a compendium of genes annotated and organized by signaling pathway was used for annotations (Ogata et al., 1998).

Semi-quantitative PCR and quantitative real-time PCR

Total RNA was prepared using the Trizol reagent (Invitrogen, Carlsbad, CA, USA). Semi-quantitative analyses were carried out as previously described (Nguyên et al., 2004). PCR products were separated on 1% agarose gels. For real-time quantitative PCR, RNA was reverse transcribed with Superscript II (Promega, Charbonnières-les-Bains, France). All PCR reactions were performed with a Stratagene X4000 thermocycler (Stratagene, Amsterdam, The Netherlands) and the SYBR Green PCR Core reagents kit (Bio-Rad, Marnes-La-Coquette, France). Experiments were performed in triplicates for each data point. Each sample was normalized on the basis of its expression of the RLP0 or B2M genes (2ΔΔCt). For amplification, the following pairs were used: SPARC 278-479: 5′-GTGCAGAGGAAACCGAA-3′ (FWD) and 5′-AAGTGGCAGGAAGAGTCGAA-3′ (REV). SPARC 1499–1709: 5′-GGTTCAAACTTTTGGGAGCA-3′ (FWD) and 5′-CCGATTCACCAACTCCAC-3′ (REV). GAPDH: 5′-ACCACCATGGAGAAGGCTGG-3′ (FWD) and 5′-CTCAGTGTAGCCCAGGATGC-3′ (REV). RPL0: 5′-GGCGACCTGGAAGTCCAACT-3′ (FWD) and 5′-CCATCAGCACCACAGCCTTC-3′ (REV). IRE1α: 5′-GCCACCCTGCAAGAGTATGT-3′ (FWD) and 5′-ATGTTGAGGGAGTGGAGGTG-3′ (REV). B2M: 5′-GTGCTGTCTCCATGTTTGATGTATC-3′ (FWD) and 5′-CTAAGTTGCCAGCCCTCCTAGA-3′ (REV), XBP1: 5′-GGAACAGCAAGTGGTAGA-3′ (FWD) and 5′-CTGGAGGGGTGACAAC-3′ (REV).

Assay for cell growth (SRB)

The SRB assay was performed as previously described (Vichai and Kirtikara, 2006). Briefly, cells were seeded into 96-well plates in 100 μl at a density of 5000 cells/well. After cell inoculation, the plates were incubated at 37℃ for 24, to 96 h. Cell were then fixed in situ with trichloroacetic acid and stained with sulforhodamine B (Sigma, St Louis, MO, USA). Absorbance was measured at 510 nm.

Statistical analyses

Data are presented as means ± s.d. or s.e.m. of at least three experiments. Statistical significance ($P<0.05$ or less) was determined using a paired or unpaired *t*-test or ANOVA as appropriate and performed with GraphPad Prism software (GraphPad Software, San Diego, CA, USA).

Acknowledgements

We thank the Chevet lab for critical reading of the manuscript. We are indebted to Sebastien Marais (Bordeaux Imaging Center, Bordeaux, France) for help with the ImageJ program.

Funding

This work was supported by the Avenir program of Institut National de la Santé et de la Recherche Médicale; Institut national du cancer; Ligue Contre le Cancer to E.C.; the French Association pour la Recherche contre le Cancer to O.P.; La Ligue contre le Cancer to N.D.; and the Cancéropôle Grand Sud-Ouest to C.G.

Supplementary material available online at
http://jcs.biologists.org/lookup/suppl/doi:10.1242/jcs.099291/-/DC1

References

Arnold, S. A. and Brekken, R. A. (2009). SPARC: a matricellular regulator of tumorigenesis. *J. Cell Commun. Signal.* **3**, 255-273.

Auf, G., Jabouille, A., Guérit, S., Pineau, R., Delugin, M., Bouchecareilh, M., Magnin, N., Favereaux, A., Maitre, M., Gaiser, T. et al. (2010). Inositol-requiring enzyme 1alpha is a key regulator of angiogenesis and invasion in malignant glioma. *Proc. Natl. Acad. Sci. USA* **107**, 15553-15558.

Barker, T. H., Baneyx, G., Cardó-Vila, M., Workman, G. A., Weaver, M., Menon, P. M., Dedhar, S., Rempel, S. A., Arap, W., Pasqualini, R. et al. (2005). SPARC regulates extracellular matrix organization through its modulation of integrin-linked kinase activity. *J. Biol. Chem.* **280**, 36483-36493.

Bouchecareilh, M., Higa, A., Fribourg, S., Moenner, M. and Chevet, E. (2011a). Peptides derived from the bifunctional kinase/RNase enzyme IRE1{alpha} modulate IRE1{alpha} activity and protect cells from endoplasmic reticulum stress. *FASEB J.* **25**, 3115-3129.

Bouchecareilh, M., Marza, E., Caruso, M. E. and Chevet, E. (2011b). Small GTPase signaling and the unfolded protein response. *Methods Enzymol.* **491**, 343-360.

Brekken, R. A. and Sage, E. H. (2001). SPARC, a matricellular protein: at the crossroads of cell-matrix communication. *Matrix Biol.* **19**, 816-827.

Calfon, M., Zeng, H., Urano, F., Till, J. H., Hubbard, S. R., Harding, H. P., Clark, S. G. and Ron, D. (2002). IRE1 couples endoplasmic reticulum load to secretory capacity by processing the XBP-1 mRNA. *Nature* **415**, 92-96.

Carrasco, D. R., Sukhdeo, K., Protopopova, M., Sinha, R., Enos, M., Carrasco, D. E., Zheng, M., Mani, M., Henderson, J., Pinkus, G. S. et al. (2007). The differentiation and stress response factor XBP-1 drives multiple myeloma pathogenesis. *Cancer Cell* **11**, 349-360.

Caruso, M. E., Jenna, S., Bouchecareilh, M., Baillie, D. L., Boismenu, D., Halawani, D., Latterich, M. and Chevet, E. (2008). GTPase-mediated regulation of the

unfolded protein response in Caenorhabditis elegans is dependent on the AAA+ ATPase CDC-48. *Mol. Cell. Biol.* **28**, 4261-4274.

Chlenski, A. and Cohn, S. L. (2010). Modulation of matrix remodeling by SPARC in neoplastic progression. *Semin. Cell Dev. Biol.* **21**, 55-65.

Drogat, B., Auguste, P., Nguyen, D. T., Bouchecareilh, M., Pineau, R., Nalbantoglu, J., Kaufman, R. J., Chevet, E., Bikfalvi, A. and Moenner, M. (2007). IRE1 signaling is essential for ischemia-induced vascular endothelial growth factor-A expression and contributes to angiogenesis and tumor growth in vivo. *Cancer Res.* **67**, 6700-6707.

Francki, A., McClure, T. D., Brekken, R. A., Motamed, K., Murri, C., Wang, T. and Sage, E. H. (2004). SPARC regulates TGF-beta1-dependent signaling in primary glomerular mesangial cells. *J. Cell. Biochem.* **91**, 915-925.

Gentleman, R. C., Carey, V. J., Bates, D. M., Bolstad, B., Dettling, M., Dudoit, S., Ellis, B., Gautier, L., Ge, Y., Gentry, J. et al. (2004). Bioconductor: open software development for computational biology and bioinformatics. *Genome Biol.* **5**, R80.

Golembieski, W. A. and Rempel, S. A. (2002). cDNA array analysis of SPARC-modulated changes in glioma gene expression. *J. Neurooncol.* **60**, 213-226.

Golembieski, W. A., Thomas, S. L., Schultz, C. R., Yunker, C. K., McClung, H. M., Lemke, N., Cazacu, S., Barker, T., Sage, E. H., Brodie, C. et al. (2008). HSP27 mediates SPARC-induced changes in glioma morphology, migration, and invasion. *Glia* **56**, 1061-1075.

Greenman, C., Stephens, P., Smith, R., Dalgliesh, G. L., Hunter, C., Bignell, G., Davies, H., Teague, J., Butler, A., Stevens, C. et al. (2007). Patterns of somatic mutation in human cancer genomes. *Nature* **446**, 153-158.

Hollien, J. and Weissman, J. S. (2006). Decay of endoplasmic reticulum-localized mRNAs during the unfolded protein response. *Science* **313**, 104-107.

Hollien, J., Lin, J. H., Li, H., Stevens, N., Walter, P. and Weissman, J. S. (2009). Regulated Ire1-dependent decay of messenger RNAs in mammalian cells. *J. Cell Biol.* **186**, 323-331.

Juin, A., Billottet, C., Moreau, V., Destaing, O., Albiges-Rizo, C., Rosenbaum, J., Génot, E. and Saltel, F. (2012). Physiological type I collagen organization induces the formation of a novel class of linear invadosomes. *Mol. Biol. Cell* **23**, 297-309.

Kunigal, S., Gondi, C. S., Gujrati, M., Lakka, S. S., Dinh, D. H., Olivero, W. C. and Rao, J. S. (2006). SPARC-induced migration of glioblastoma cell lines via uPA-uPAR signaling and activation of small GTPase RhoA. *Int. J. Oncol.* **29**, 1349-1357.

Lee, K., Tirasophon, W., Shen, X., Michalak, M., Prywes, R., Okada, T., Yoshida, H., Mori, K. and Kaufman, R. J. (2002). IRE1-mediated unconventional mRNA splicing and S2P-mediated ATF6 cleavage merge to regulate XBP1 in signaling the unfolded protein response. *Genes Dev.* **16**, 452-466.

Liu, D. Y., Martic, M., Clarke, G. N., Dunlop, M. E. and Baker, H. W. (1999). An important role of actin polymerization in the human zona pellucida-induced acrosome reaction. *Mol. Hum. Reprod.* **5**, 941-949.

Marciniak, S. J. and Ron, D. (2006). Endoplasmic reticulum stress signaling in disease. *Physiol. Rev.* **86**, 1133-1149.

Moenner, M., Pluquet, O., Bouchecareilh, M. and Chevet, E. (2007). Integrated endoplasmic reticulum stress responses in cancer. *Cancer Res.* **67**, 10631-10634.

Moreau, V., Tatin, F., Varon, C. and Génot, E. (2003). Actin can reorganize into podosomes in aortic endothelial cells, a process controlled by Cdc42 and RhoA. *Mol. Cell. Biol.* **23**, 6809-6822.

Nguyên, D. T., Kebache, S., Fazel, A., Wong, H. N., Jenna, S., Emadali, A., Lee, E. H., Bergeron, J. J., Kaufman, R. J., Larose, L. et al. (2004). Nck-dependent activation of extracellular signal-regulated kinase-1 and regulation of cell survival during endoplasmic reticulum stress. *Mol. Biol. Cell* **15**, 4248-4260.

Ogata, H., Goto, S., Fujibuchi, W. and Kanehisa, M. (1998). Computation with the KEGG pathway database. *Biosystems* **47**, 119-128.

Oikawa, D., Tokuda, M. and Iwawaki, T. (2007). Site-specific cleavage of CD59 mRNA by endoplasmic reticulum-localized ribonuclease, IRE1. *Biochem. Biophys. Res. Commun.* **360**, 122-127.

Oikawa, D., Tokuda, M., Hosoda, A. and Iwawaki, T. (2010). Identification of a consensus element recognized and cleaved by IRE1 alpha. *Nucleic Acids Res.* **38**, 6265-6273.

Papandreou, I., Denko, N. C., Olson, M., Van Melckebeke, H., Lust, S., Tam, A., Solow-Cordero, D. E., Bouley, D. M., Offner, F., Niwa, M. et al. (2011). Identification of an Ire1alpha endonuclease specific inhibitor with cytotoxic activity against human multiple myeloma. *Blood* **117**, 1311-1314.

Parsons, D. W., Jones, S., Zhang, X., Lin, J. C., Leary, R. J., Angenendt, P., Mankoo, P., Carter, H., Siu, I. M., Gallia, G. L. et al. (2008). An integrated genomic analysis of human glioblastoma multiforme. *Science* **321**, 1807-1812.

Pellegrin, S. and Mellor, H. (2007). Actin stress fibres. *J. Cell Sci.* **120**, 3491-3499.

Podhajcer, O. L., Benedetti, L. G., Girotti, M. R., Prada, F., Salvatierra, E. and Llera, A. S. (2008). The role of the matricellular protein SPARC in the dynamic interaction between the tumor and the host. *Cancer Metastasis Rev.* **27**, 691-705.

Rempel, S. A., Golembieski, W. A., Fisher, J. L., Maile, M. and Nakeff, A. (2001). SPARC modulates cell growth, attachment and migration of U87 glioma cells on brain extracellular matrix proteins. *J. Neurooncol.* **53**, 149-160.

Ridley, A. J., Paterson, H. F., Johnston, C. L., Diekmann, D. and Hall, A. (1992). The small GTP-binding protein rac regulates growth factor-induced membrane ruffling. *Cell* **70**, 401-410.

Ridley, A. J., Allen, W. E., Peppelenbosch, M. and Jones, G. E. (1999). Rho family proteins and cell migration. *Biochem. Soc. Symp.* **65**, 111-123.

Romero-Ramirez, L., Cao, H., Nelson, D., Hammond, E., Lee, A. H., Yoshida, H., Mori, K., Glimcher, L. H., Denko, N. C., Giaccia, A. J. et al. (2004). XBP1 is essential for survival under hypoxic conditions and is required for tumor growth. *Cancer Res.* **64**, 5943-5947.

Schröder, M. and Kaufman, R. J. (2005). The mammalian unfolded protein response. *Annu. Rev. Biochem.* **74**, 739-789.

Schultz, C., Lemke, N., Ge, S., Golembieski, W. A. and Rempel, S. A. (2002). Secreted protein acidic and rich in cysteine promotes glioma invasion and delays tumor growth in vivo. *Cancer Res.* **62**, 6270-6277.

Seno, T., Harada, H., Kohno, S., Teraoka, M., Inoue, A. and Ohnishi, T. (2009). Downregulation of SPARC expression inhibits cell migration and invasion in malignant gliomas. *Int. J. Oncol.* **34**, 707-715.

Shuda, M., Kondoh, N., Imazeki, N., Tanaka, K., Okada, T., Mori, K., Hada, A., Arai, M., Wakatsuki, T., Matsubara, O. et al. (2003). Activation of the ATF6, XBP1 and grp78 genes in human hepatocellular carcinoma: a possible involvement of the ER stress pathway in hepatocarcinogenesis. *J. Hepatol.* **38**, 605-614.

Sweetwyne, M. T., Brekken, R. A., Workman, G., Bradshaw, A. D., Carbon, J., Siadak, A. W., Murri, C. and Sage, E. H. (2004). Functional analysis of the matricellular protein SPARC with novel monoclonal antibodies. *J. Histochem. Cytochem.* **52**, 723-733.

Tai, I. T. and Tang, M. J. (2008). SPARC in cancer biology: its role in cancer progression and potential for therapy. *Drug Resist. Updat.* **11**, 231-246.

Thomas, S. L., Alam, R., Lemke, N., Schultz, L. R., Gutiérrez, J. A. and Rempel, S. A. (2010). PTEN augments SPARC suppression of proliferation and inhibits SPARC-induced migration by suppressing SHC-RAF-ERK and AKT signaling. *Neuro-oncol.* **12**, 941-955.

Vichai, V. and Kirtikara, K. (2006). Sulforhodamine B colorimetric assay for cytotoxicity screening. *Nat. Protoc.* **1**, 1112-1116.

Welihinda, A. A., Tirasophon, W., Green, S. R. and Kaufman, R. J. (1998). Protein serine/threonine phosphatase Ptc2p negatively regulates the unfolded-protein response by dephosphorylating Ire1p kinase. *Mol. Cell. Biol.* **18**, 1967-1977.

Xue, Z., He, Y., Ye, K., Gu, Z., Mao, Y. and Qi, L. (2011). A conserved structural determinant located at the interdomain region of mammalian inositol-requiring enzyme 1alpha. *J. Biol. Chem.* **286**, 30859-30866.

Yoshida, H., Matsui, T., Yamamoto, A., Okada, T. and Mori, K. (2001). XBP1 mRNA is induced by ATF6 and spliced by IRE1 in response to ER stress to produce a highly active transcription factor. *Cell* **107**, 881-891.

Yoshida, H., Matsui, T., Hosokawa, N., Kaufman, R. J., Nagata, K. and Mori, K. (2003). A time-dependent phase shift in the mammalian unfolded protein response. *Dev. Cell* **4**, 265-271.